

Coherent population trapping in a dressed two-level atom via a bichromatic field

Peng Li^{1,2}, Xi-Jing Ning³, Qun-Zhang² and J Q You¹

¹Department of Physics and Surface Physics Laboratory (National Key Laboratory), Fudan University, Shanghai 200433, China

²Department of Materials Science, Fudan University, Shanghai 200433, China

³Institute of Modern Physics and the Key Lab of Applied Ion Beam Physics of the Ministry of Education, Fudan University, Shanghai 200433, China

E-mail: lipeng@fudan.edu.cn, jqyou@fudan.edu.cn

Abstract. We show theoretically that by applying a bichromatic electromagnetic field, the dressed states of a monochromatically driven two-level atom can be pumped into a coherent superposition termed as dressed-state coherent population trapping. Such effect can be viewed as a new doorknob to manipulate a two-level system via its control over dressed-state populations. Application of this effect in the precision measurement of Rabi frequency, the unexpected population inversion and lasing without inversion are discussed to demonstrate such controllability.

PACS numbers: 42.50.Hz, 32.80.Qk

1. Introduction

As unveiled by the remarkable suppression of fluorescence, coherent population trapping (CPT) [1] has been regarded as a significant demonstration of macroscopic quantum coherence and interference. The importance of CPT is well illuminated by its numerous applications in laser cooling, stimulated Raman adiabatic passage (STIRAP) [2], electromagnetically induced transparency (EIT) [3], and lasing without inversion (LWI) [4]. Recent studies even extend the concept of CPT beyond optics to the realm of electron transportation in coupled quantum dots, where an all-electronic analogy of CPT emerges with potential values for current rectification [5].

In general, CPT is realized within a driven Λ -type atom, in which a *dark state* is prepared via the field-induced coherent superposition of the two lower atomic states. The mixing ratio of this superposition is self-adjusted to have the two transition paths from the lower states to the upper state interfere destructively, so that excitation to the upper state is forbidden. Therefore, suppression of fluorescence from the upper state results in a striking darkline at the vicinity of two-photon resonance [6]. Since CPT by its nature relies on the coherence between the two lower atomic states, it is vulnerable to any mechanism which may destroy this coherence. For this reason, CPT is predominantly studied in bare Λ -type atoms with negligible spontaneous transition between the two lower states.

In many cases the dressed-atom picture provides a unique insight in dealing with atom-photon interaction problems [7, 8]. A well-known example is the Rabi splitting of a monochromatically driven two-level atom (TLA), where the Rabi doublet can be well treated as eigenstates of the (semiclassical) atom-field interaction Hamiltonian, i.e., *dressed states* (DSs). When driving field is modeled quantum-mechanically, a ladder of such dressed-state doublets (DSDs) emerges with quasi-equidistant energy spacing between adjacent DSDs. Coherent transition between DSs within each DSD is forbidden due to vanishing dipole moment [9]. To induce coherence in the DS basis one needs to couple adjacent DSDs, where transitions are allowed between DSs associated with different DSDs [9]. Such coherent transitions between DSs result in an interesting spectral signature of the underlying atom-field interaction, and novel effects such as spectral cancellation of spontaneous emission can be realized (see, the *doubly dressed-atom* in [10]).

In contrast to [10], we show in this paper that it is also possible to achieve a CPT-like coherence *within* each DSD, via a bichromatic field which couples the two DSs to an auxiliary atomic state. We show that such a dressed-state coherent population trapping (DSCPT) is formed in analogy to the conventional CPT in bare atomic basis. As expected, the occurrence of such DSCPT is reflected in a sharp suppression of fluorescence from the auxiliary state. Our analytical and numerical studies show that the efficiency of DSCPT is limited by its rate of decoherence, i.e., the rate of spontaneous decay of the TLA (see Section 2 for details). Practically, DSCPT can be viewed as a new doorknob to manipulate a TLA due to its ability to control the DS populations. Application

of DSCPT in the Autler-Townes spectroscopy leads to an enhanced precision in the measurement of Rabi frequency. DSCPT can also be used to obtain an unexpected population inversion for a driven TLA, where the previously reported *dynamically induced irreversibility* [11] can be treated as a limiting case within this context, which provides us a new picture in understanding the origin of this phenomenon. Additionally, novel LWI effects with and without hidden inversion are also presented to demonstrate the versatile controllability provided by DSCPT (see Section 3 for details).

We wish to emphasize that DSCPT is different from the CPT investigated in a degenerate two-level atom (DTLA) [13], where effects of Zeeman sublevels are investigated. In a DTLA, sublevels of the ground (excited) level do not contain any contamination from the excited (ground) level, with or without external magnetic field. While in a coherently driven TLA, each DS is a coherent mixing of the ground state and the excited state. Therefore, the coherence between DSs discussed here intrinsically differs from that studied in [13].

This paper is organized as follows: In Section 2, we introduce the theoretical model and provide both analytical and numerical investigation of DSCPT. In Section 3, we demonstrate the application of DSCPT via three examples. Finally, a brief summary is given in Section 4.

2. Demonstration of dressed-state coherent population trapping

2.1. Model and theoretical analysis

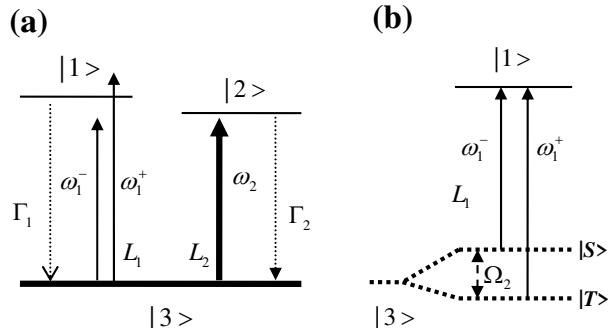


Figure 1. Schematic diagram of a V-type three-level atom driven by two externally applied electromagnetic fields. (a) The $|1\rangle - |3\rangle$ transition of the V-type atom is driven by a weak bichromatic field L_1 , while the $|2\rangle - |3\rangle$ transition is driven by a strong monochromatic field L_2 . (b) An effective Λ -type atom formed in (a), where $|S\rangle$ and $|T\rangle$ are the DSs of the subsystem composed of transition $|2\rangle - |3\rangle$ and field L_2 .

The theoretical model we study is a V-type atom [see Fig. 1(a)]. The $|1\rangle - |3\rangle$ transition is driven by a weak bichromatic field L_1 , while the $|2\rangle - |3\rangle$ transition is driven by a strong monochromatic field L_2 . The angular frequencies corresponding to these two transitions are ω_{13} and ω_{23} , respectively. The two driving fields L_1 and L_2 are expressed as $E_1(t) = \frac{1}{2}E_1^+ \cdot e^{i\omega_1^+ t} + \frac{1}{2}E_1^- \cdot e^{i\omega_1^- t} + \text{H.c}$ and $E_2(t) = \frac{1}{2}E_2 \cdot e^{i\omega_2 t} + \text{H.c}$, where

$\omega_1^\pm = \omega_1 \pm \delta$ denote the two frequencies of the bichromatic field L_1 and ω_2 is the frequency of the monochromatic field L_2 . Thus we can define two detunings $\Delta_1 = \omega_{13} - \omega_1$ and $\Delta_2 = \omega_{23} - \omega_2$. The Rabi frequencies associated with the two atomic transitions can be written as $\Omega_1^\pm = E_1^\pm \cdot \mu_{13}/\hbar$ and $\Omega_2 = E_2 \cdot \mu_{23}/\hbar$, where $\mu_{13}(\mu_{23})$ denotes the dipole moment of the $|1\rangle - |3\rangle$ ($|2\rangle - |3\rangle$) transition. The rate of spontaneous decay from $|1\rangle$ ($|2\rangle$) to $|3\rangle$ is denoted as $\Gamma_1(\Gamma_2)$. In what follows, the field amplitudes E_1^\pm and E_2 , the dipole moments μ_{13} and μ_{23} , and the Rabi frequencies Ω_1^\pm and Ω_2 are chosen as real numbers for simplicity, without loss of generality.

First let us look at the system as if L_1 is absent. It is obvious that L_2 plus $|2\rangle - |3\rangle$ transition correspond to a standard driven TLA [14]. The semiclassical DSs are the eigenstates of the Hamiltonian (in the rotating-wave frame, $\hbar = 1$) $H_{\text{TLA}} = \Delta_2|\tilde{2}\rangle\langle\tilde{2}| + \frac{1}{2}\Omega_2(|\tilde{3}\rangle\langle\tilde{2}| + |\tilde{2}\rangle\langle\tilde{3}|)$, i.e.,

$$\begin{aligned} |S\rangle &= \sin\chi|\tilde{3}\rangle + \cos\chi|\tilde{2}\rangle, \\ |T\rangle &= \cos\chi|\tilde{3}\rangle - \sin\chi|\tilde{2}\rangle, \end{aligned} \quad (1)$$

where $\chi = \frac{1}{2}\tan^{(-1)}(\Omega_2/\Delta_2)$, $|\tilde{2}\rangle = |2\rangle e^{-i\omega_2 t}$, and $|\tilde{3}\rangle = |3\rangle$. And the corresponding eigenenergies are $E_{S,T} = \frac{1}{2}\Delta_2 \pm \frac{1}{2}\sqrt{\Delta_2^2 + \Omega_2^2}$, with $G = \sqrt{\Delta_2^2 + \Omega_2^2}$ being the Rabi-splitting. (We emphasize that both the ground state $|3\rangle$ and the upper state $|2\rangle$ are splitted into doublet via the atom-field interaction. Without specific notation, we refer $|S\rangle$ and $|T\rangle$ to the field-induced doublet associated with the ground state $|3\rangle$, for the rest of this paper.) Meanwhile, the quantum mechanical DSs are the eigenstates of the Hamiltonian $\mathcal{H}'_{\text{TLA}} = \Delta_2|3, n\rangle\langle 3, n| + g\sqrt{n}(|3, n\rangle\langle 2, n-1| + \text{H.c.})$, i.e.,

$$\begin{aligned} |S_n\rangle &= \sin\chi'|3, n\rangle + \cos\chi'|2, n-1\rangle, \\ |T_n\rangle &= \cos\chi'|3, n\rangle - \sin\chi'|2, n-1\rangle, \end{aligned} \quad (2)$$

where $\chi' = \frac{1}{2}\tan^{(-1)}(2g\sqrt{n}/\Delta_2)$, with $|n\rangle$ and g being the Fock state of the field and the coupling strength between the field and the atom, respectively. Since the classical field L_2 is not in a pure Fock state $|n\rangle$ but a coherent state with average photon number \bar{n} , the correspondence between semiclassical Rabi frequency and the field's photon number leads to $\Omega_2 = 2g\sqrt{\bar{n}}$.

To achieve CPT in the above DS basis one needs to construct an effective Λ -type atom. This can be fulfilled by introducing the bichromatic field L_1 , whose center frequency is (near) resonant with $|1\rangle - |3\rangle$ transition, as shown in Fig. 1(a). The two transitions $|1\rangle - |T\rangle$ and $|1\rangle - |S\rangle$ are then coupled by the two frequency components ω_1^+ and ω_1^- of L_1 , respectively, as shown in Fig. 1(b). Since both $|S\rangle$ and $|T\rangle$ are contaminated by bare state $|3\rangle$, the effective dipole moments corresponding to transitions $|1\rangle - |S\rangle$ and $|1\rangle - |T\rangle$ can easily be deduced from Eq. (1) as $\mu_{1S} = \langle 1|\vec{\mathcal{D}}|S\rangle = \mu_{13}\sin\chi$ and $\mu_{1T} = \langle 1|\vec{\mathcal{D}}|T\rangle = \mu_{13}\cos\chi$. Neglecting the non-resonant terms (which involves a second RWA), i.e., the coupling between the field component ω_1^+ and $|1\rangle - |S\rangle$ transition, and that between ω_1^- and $|1\rangle - |T\rangle$ transition, the Rabi frequencies associated with these two transitions are simply $\Omega_S = \Omega_1^+ \sin\chi$ and $\Omega_T = \Omega_1^+ \cos\chi$. Accordingly, the Hamiltonian

of the effective Λ -type atom in Fig. 1(b) can be written as

$$H_\Lambda = \frac{1}{2} \left[\Omega_S |\tilde{1}\rangle \langle \tilde{S}| + \Omega_T |\tilde{1}\rangle \langle \tilde{T}| + \text{H.c.} \right] + \Delta |\tilde{1}\rangle \langle \tilde{1}| + \Delta_{2\text{photon}} |\tilde{S}\rangle \langle \tilde{S}|, \quad (3)$$

where $\Delta = \omega_{13} - E_T - \omega_1^+$, $\Delta_{2\text{photon}} = (E_S - E_T) - (\omega_1^+ - \omega_1^-)$, $|\tilde{1}\rangle = e^{-i\omega_1^+ t} |1\rangle$, $|\tilde{S}\rangle = e^{-i(\omega_1^+ - \omega_1^-)t} |S\rangle$, and $|\tilde{T}\rangle = |T\rangle$. As essential for CPT, the two-photon resonance condition requires that $(E_S - E_T) - (\omega_1^+ - \omega_1^-) = 0$, i.e.,

$$G = 2\delta, \quad (4)$$

which can fulfilled by manipulating either L_1 or L_2 , via tuning 2δ or G , respectively.

Once Eq.(4) is satisfied, it is routine to show that both dark and bright states exist in this effective Λ -type atom. We adopt the terminology in [1], i.e., the noncoupled and coupled states, which are defined as

$$|NC\rangle = \cos \theta |\tilde{S}\rangle - \sin \theta |\tilde{T}\rangle = e^{-i2\delta t} \cos \theta |S\rangle - \sin \theta |T\rangle, \quad (5)$$

and

$$|C\rangle = \sin \theta |\tilde{S}\rangle + \cos \theta |\tilde{T}\rangle = e^{-i2\delta t} \sin \theta |S\rangle + \cos \theta |T\rangle, \quad (6)$$

where $\theta = \tan^{-1}(\Omega_S/\Omega_T)$. Since $\langle 1|H'_\Lambda|NC\rangle = 0$, an atom in the noncoupled state $|NC\rangle$ cannot be excited to $|1\rangle$ by absorbing L_1 photons. On the other hand, since $K = \|\langle 1|H'_\Lambda|C\rangle\| = \frac{1}{2}\sqrt{\Omega_S^2 + \Omega_T^2} > 0$, there is nonzero probability for an atom in the coupled state $|C\rangle$ to be excited to $|1\rangle$. In contrast to the excitation paths, the spontaneous decay processes for $|1\rangle \rightarrow |NC\rangle$ and $|1\rangle \rightarrow |C\rangle$ do not contain such a clear-cut asymmetry. The decay rates associated with $|1\rangle \rightarrow |C\rangle$ and $|1\rangle \rightarrow |NC\rangle$ are proportional to the square of their corresponding dipole moments, i.e., $\Gamma_{1 \rightarrow NC} = (\sin^2 \chi \cos^2 \theta + \cos^2 \chi \sin^2 \theta) \Gamma_1$, and $\Gamma_{1 \rightarrow C} = (\sin^2 \chi \sin^2 \theta + \cos^2 \chi \cos^2 \theta) \Gamma_1$. Take $\chi = \theta = \pi/4$ as an example, for which $\Gamma_{1 \rightarrow NC} = \Gamma_{1 \rightarrow C} = \Gamma_1/2$, it is clear that one pump-decay cycle $|C\rangle \rightarrow |1\rangle \rightarrow |C\rangle$ or $|NC\rangle$ will transfer half of the population of $|C\rangle$ into $|NC\rangle$. After several pump-decay cycles, most atomic population will be trapped in $|NC\rangle$, i.e., DSCPT is obtained.

It should be noted that $|NC\rangle$ itself is not radiatively stable, due to the spontaneous decay from $|2\rangle$ to $|3\rangle$. To demonstrate this more explicitly we resort to the fully-quantized correspondence of the semiclassical noncoupled state $|NC\rangle$, i.e.,

$$|NC'_n\rangle = \cos \theta |S_n\rangle - \sin \theta |T_n\rangle. \quad (7)$$

As shown in Ref. [9], $|S_n\rangle$ and $|T_n\rangle$ spontaneously decay to the next low-lying doublet composed of $|S_{n-1}\rangle$ and $|T_{n-1}\rangle$, by emitting a reservoir photon whose frequency is centered at ω_{23} . Each spontaneous emission event (quantum jump) completely destroys the coherence of $|NC'_n\rangle$, so that the decoherence rate of $|NC'_n\rangle$ is equivalent to the frequency of occurrence of such quantum jumps, i.e., the spontaneous decay rate Γ_2 of state $|2\rangle$. Nevertheless, if $K \gg \Gamma_2$ and $\Gamma_{1 \rightarrow NC} \gg \Gamma_2$, then after each $|2\rangle \rightarrow |3\rangle$

quantum jump, the DS coherence will be quickly reestablished in $|NC'_{n-1}\rangle$ within a time scale much smaller than the average time interval between two successive quantum jumps. In this sense $|NC\rangle$ can be viewed as quasi-stable and we say that an effective DSCPT occurs. Therefore, we expect to see fluorescence suppression from $|1\rangle$ and the population divergence between $|NC\rangle$ and $|C\rangle$ at the vicinity of two-photon resonance, as two symbolic manifestations for DSCPT.

Next we give a numerical calculation of DSCPT under the bare atomic state basis, using a semiclassical master equation (see, e.g., [15, 16, 17]). In contrast to the theoretical analysis above, the numerical method we use does not require a second RWA, so the calculations are valid even when the driving fields are tuned far away from the two-photon resonance condition (4).

2.2. Numerical calculation

For the model scheme shown in Fig. 1(a) the semiclassical Hamiltonian can be written as (with RWA)

$$H = \begin{bmatrix} \Delta_1 & 0 & \frac{1}{2}\Omega_1^+ e^{-i\delta t} + \frac{1}{2}\Omega_1^- e^{i\delta t} \\ 0 & \Delta_2 & \frac{1}{2}\Omega_2 \\ \frac{1}{2}\Omega_1^+ e^{i\delta t} + \frac{1}{2}\Omega_1^- e^{-i\delta t} & \frac{1}{2}\Omega_2 & 0 \end{bmatrix}. \quad (8)$$

The master equation governing the time evolution of atomic populations and coherences can be obtained by combining the reversible Liouville-equation $i\dot{\rho} = [H, \rho]$ with relevant irreversible relaxation parameters, as,

$$\dot{x}(t) = [A^- e^{-i\delta t} + A^0 + A^+ e^{i\delta t}] x(t) + e^{-i\delta t} V^- + V^0 + e^{i\delta t} V^+. \quad (9)$$

In Eq. (9), V^0 , V^\pm , and $x(t)$ are 8×1 column vectors defined as $V^0 = [\frac{1}{2}i\Omega_2, 0, -\frac{1}{2}i\Omega_2, 0, 0, 0, 0, 0]^T$, $V^+ = [0, \frac{1}{2}i\Omega_1^-, 0, 0, 0, -\frac{1}{2}i\Omega_1^+, 0, 0]^T$, $V^- = [0, \frac{1}{2}i\Omega_1^+, 0, 0, 0, -\frac{1}{2}i\Omega_1^-, 0, 0]^T$ and $x(t) = [x_1(t), \dots, x_8(t)]^T$, where $x_1(t) = \rho_{23}$, $x_2(t) = \rho_{13}$, $x_3(t) = \rho_{32}$, $x_4(t) = \rho_{22}$, $x_5(t) = \rho_{12}$, $x_6(t) = \rho_{31}$, $x_7(t) = \rho_{21}$, and $x_8(t) = \rho_{11}$. The notations A^\pm and A^0 are 8×8 matrices defined as $A_{11}^0 = i\Delta_2 - \gamma_{23}$, $A_{22}^0 = i\Delta_1 - \gamma_{13}$, $A_{33}^0 = -i\Delta_2 - \gamma_{23}$, $A_{44}^0 = -\Gamma_2$, $A_{55}^0 = i(\Delta_1 - \Delta_2) - \gamma_{12}$, $A_{66}^0 = -i\Delta_1 - \gamma_{13}$, $A_{77}^0 = i(\Delta_2 - \Delta_1) - \gamma_{12}$, $A_{88}^0 = -\Gamma_1$, $A_{43}^0 = A_{76}^0 = A_{67}^0 = A_{38}^0 = \frac{1}{2}i\Omega_2$, $A_{14}^0 = -i\Omega_2$, $A_{41}^0 = A_{52}^0 = A_{25}^0 = A_{18}^0 = -\frac{1}{2}i\Omega_2$, $A_{34}^0 = i\Omega_2$, $A_{71}^+ = A_{82}^+ = -\frac{1}{2}i\Omega_1^-$, $A_{24}^+ = A_{17}^+ = -\frac{1}{2}i\Omega_1^+$, $A_{64}^+ = A_{35}^+ = \frac{1}{2}i\Omega_1^-$, $A_{53}^+ = A_{86}^+ = \frac{1}{2}i\Omega_1^+$, $A_{28}^+ = -i\Omega_1^+$, $A_{68}^+ = i\Omega_1^-$, $A_{71}^- = A_{82}^- = -\frac{1}{2}i\Omega_1^+$, $A_{24}^- = A_{17}^- = -\frac{1}{2}i\Omega_1^-$, $A_{64}^- = A_{35}^- = \frac{1}{2}i\Omega_1^+$, $A_{53}^- = A_{86}^- = \frac{1}{2}i\Omega_1^-$, $A_{28}^- = -i\Omega_1^-$, $A_{68}^- = i\Omega_1^+$, where $\gamma_{12} = (\Gamma_1 + \Gamma_2)/2$, $\gamma_{13} = \Gamma_1/2$ and $\gamma_{23} = \Gamma_2/2$ are the damping rates of atomic coherences. The remaining matrix elements of A^\pm and A^0 are zeros. Note that in deriving Eq. (9) we have used $\rho_{11} + \rho_{22} + \rho_{33} = 1$ to eliminate ρ_{33} .

By decomposing $x(t)$ into a harmonic expansion $x(t) = \sum_{n=-\infty}^{\infty} x^{(n)}(t)e^{i\delta t}$, Eq.(9) can be recast into an recursive relation

$$\begin{aligned} \dot{x}^{(n)}(t) &= [A^0 - in\delta I] x^{(n)}(t) + A^- x^{(n+1)}(t) \\ &+ A^+ x^{(n-1)}(t) + V^- \delta_{n,-1} + V^0 \delta_{n,0} + V^+ \delta_{n,1}, \end{aligned} \quad (10)$$

where I denotes a 8×8 unit matrix. In steady state, $\dot{x}^{(n)}(t) = 0$, which gives the steady-state solution of $x(t)$ below:

$$\begin{bmatrix} \cdots \\ M_{-2} & -A^- \\ -A^+ & M_{-1} & -A^- \\ & -A^+ & M_0 & -A^- \\ & & -A^+ & M_1 & -A^- \\ & & & -A^+ & M_2 \\ & & & & \cdots \end{bmatrix} \begin{bmatrix} \cdots \\ x^{(-2)}(\infty) \\ x^{(-1)}(\infty) \\ x^{(0)}(\infty) \\ x^{(1)}(\infty) \\ x^{(2)}(\infty) \\ \cdots \end{bmatrix} = \begin{bmatrix} \cdots \\ 0 \\ V^- \\ V^0 \\ V^+ \\ 0 \\ \cdots \end{bmatrix}, \quad (11)$$

where $M_n = in\delta I - A^0$. In this way we can calculate the steady-state atomic density matrix by truncating Eq. (11) at a given order with desired numerical precision. Moreover, using Eq. (5) and (6), the steady-state population in the $|NC\rangle$ and $|C\rangle$ can be calculated from the solution of (11) straightforwardly. As an example for $\chi = \theta = \pi/4$, the steady-state populations of $|NC\rangle$ and $|C\rangle$ are

$$\begin{aligned} \rho_{NC,NC}^{(0)}(\infty) &= \frac{1}{2} \left[1 - x_8^{(0)}(\infty) + x_4^{(2)}(\infty) + x_4^{(-2)}(\infty) \right] \\ &+ \frac{1}{4} \left[x_8^{(-2)}(\infty) - x_3^{(-2)}(\infty) + x_1^{(-2)}(\infty) \right] \\ &+ \frac{1}{4} \left[x_8^{(2)}(\infty) + x_3^{(2)}(\infty) - x_1^{(2)}(\infty) \right] \end{aligned} \quad (12)$$

and

$$\rho_{C,C}^{(0)}(\infty) = 1 - \rho_{NC,NC}^{(0)}(\infty) - x_8^0(\infty) \quad (13)$$

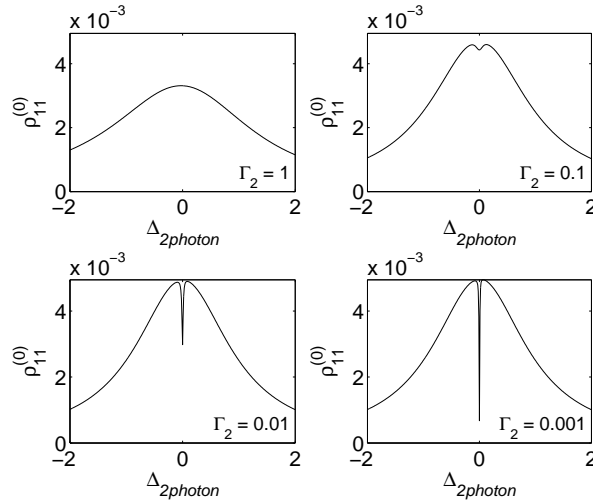


Figure 2. The steady-state population of state $|1\rangle$ as a function of two-photon detuning $\Delta_{2\text{photon}}$. Here we choose $\delta = 5$, $\Delta_1 = \Delta_2 = 0$, and $\Omega_1^+ = \Omega_1^- = 0.1$, so that $\chi = \theta = \pi/4$. The detuning $\Delta_{2\text{photon}}$ is realized via variation of Ω_2 , and all relevant parameters are normalized with respect to Γ_1 .

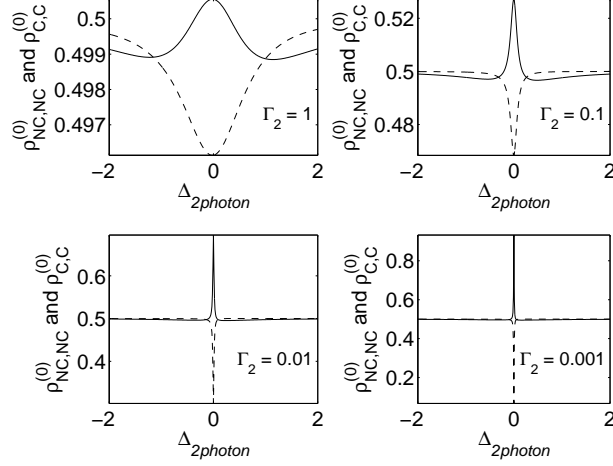


Figure 3. The steady-state population in the noncoupled state $|NC\rangle$ (solid line) and the coupled state $|C\rangle$ (dashed line) as a function of two-photon detuning $\Delta_{2\text{photon}}$. Here all parameters are the same as in Fig. 2.

In real calculations, we use $\Gamma_1 = 1$ and normalize all parameters with respect to Γ_1 . Also, we specifically choose $\Delta_2 = 0$ and $\Omega_1^+ = \Omega_1^-$, to have $\chi = \theta = \pi/4$ for simplicity. In Fig. 2 we show the steady-state population $\rho_{11}^{(0)} = x_8^{(0)}(\infty)$ of state $|1\rangle$, as a function of two-photon detuning $\Delta_{2\text{photon}} = \Omega_2 - 2\delta$ (since $\Delta_2 = 0$). Other parameters are chosen as $\Delta_1 = 0$, $\Omega_1^+ = \Omega_1^- = 0.1$, $\delta = 5$, and $\Delta_{2\text{photon}}$ is varied through Ω_2 . From Fig. 2 we see that, as Γ_2 decreases from 1 to 0.001, the darkline appears at $\Delta_{2\text{photon}} = 0$ and gradually becomes apparent. We also display in Fig. 3 the steady-state populations of $|NC\rangle$ and $|C\rangle$, using the same parameters as in Fig. 2. For small Γ_2 , populations of $|NC\rangle$ and $|C\rangle$ demonstrate clear divergence at two-photon resonance, although they are almost equally distributed at nonresonant places. The numerical results also confirms that DSCPT is most effective for the parameter range $K \gg \Gamma_2$ and $\Gamma_1 \gg \Gamma_2$, as demonstrated in Fig. 2(c) and Fig. 2(d), as well as in Fig. 3(c) and Fig. 3(d). We note that the widths of the central dips and peaks in Fig. 2 and Fig. 3 are in general slightly greater than Γ_2 due to the power broadening introduced by L_1 . As a summary of numerical calculations we conclude that the parameter's range pertinent to DSCPT can be given as $\Omega_2 \gg K \gg \Gamma_2$, and $\Gamma_1 \gg \Gamma_2$.

3. Applications

In this section we provide three examples on the application of DSCPT. Throughout the discussions we refer a driven TLA to the subsystem composed of transition $|2\rangle - |3\rangle$ and field L_2 . The DSCPT via inclusion of state $|1\rangle$ and field L_1 is thus viewed as an artificial control over the driven TLA. Moreover, all relevant parameters are normalized with respect to Γ_1 as in the previous section.

3.1. Precision measurement of Rabi frequency

The absolute Rabi frequency is the product of the field strength and the associated atomic dipole moment. Knowing either one, the measurement of Rabi frequency reveals the other. Thus the precision measurement of Rabi frequency is of great importance in laser and atomic spectroscopy. The usual measurement of Rabi frequency invokes the Autler-Townes (AT) spectroscopy, in which the Rabi splitting of a resonantly driven TLA is probed by a second *monochromatic* field which couples the ground state $|3\rangle$ to a probe state $|1\rangle$. The variation of the fluorescence intensity from $|1\rangle$ with respect to the detuning of the probe field reveals an AT doublet. Spectroscopic measurement of the frequency splitting of the AT doublet directly gives the Rabi frequency Ω_2 .

The weakness of this conventional setup lies in that each absorption peak of the AT doublet possesses an intrinsic linewidth (for, e.g., $\chi = \pi/4$)

$$W_{AT} = \frac{1}{2}\Gamma_2 + \Gamma_1, \quad (14)$$

which obviously depends on the spectral width of state $|1\rangle$. This means that the introduction of a probe state inevitably produces an additional measuring error Γ_1 . As far as monochromatic probe field is concerned, this error is unremovable and the only way to reduce it is to choose a probe state with a longer lifetime, which on the other hand leads to a longer photon collection time and therefore deteriorates the signal-to-noise ratio.

However, by using a *bichromatic* probe field as described in the previous discussion of DSCPT, the above difficulty can be circumvented. The Rabi frequency Ω_2 can be alternatively measured through the internal frequency difference of the bichromatic probe field, since the position of fluorescence darkline (as shown in Fig.2) corresponds to the equality $\Omega_2 = 2\delta$. Because the width of the dark resonance is independent of Γ_1 , Ω_2 can be measured with a precision invulnerable to the choice of the probe state. Although this precision is still plagued by the L_1 field-induced power broadening, it can be made sufficiently smaller than Γ_1 by reducing the intensity of the bichromatic field L_1 to satisfy $K \ll \Gamma_1$. Therefore, this method would be superior to the conventional AT spectroscopy whenever the spectral width of the probe state is much larger than that of the atomic transition to be measured.

3.2. Unexpected population inversion

It is well known that no steady-state population inversion exists for a driven TLA [18]. Sustained population inversion can be realized in multi-level atoms where irreversible population transfer channels between excited states come into play. For example, if an additional $|1\rangle \rightarrow |2\rangle$ decay channel is open for the V-type atom shown in Fig. 1(a), a steady-state inversion on the $|2\rangle - |3\rangle$ transition can be achieved with appropriate parameter setup. However, even when no such decay channel is available, artificial population transfer in the DS basis can still lead to an unexpected inversion for the $|2\rangle - |3\rangle$ transition, which is termed as *dynamically-induced irreversibility* by Meduri *et*

al [11]. In Section 2 we have seen that with ideal DSCPT ($\rho_{NC,NC} \approx 1$) the atomic population is trapped in the dark state $|NC\rangle$, thus the mixing angle θ provides an independent doorknob on the DS populations. Next we show that the unexpected inversion can be realized via DSCPT as well, and the results in [11] can be viewed as a limiting case of this method.

As shown in a rate-equation approach [19], the DS populations of a monochromatically driven TLA obey

$$\frac{\rho_{SS}}{\rho_{TT}} = \tan^4 \chi, \quad (15)$$

which leads to $\rho_{SS} \leq \rho_{TT}$ because $0 \leq \chi \leq \pi/4$, i.e., the DS population is always non-inverted. Furthermore, from Eq.(1) one finds

$$\rho_{22} - \rho_{33} = \cos 2\chi \cdot (\rho_{SS} - \rho_{TT}). \quad (16)$$

Due to the nonnegativity of $\cos 2\chi$, a DS inversion always corresponds to a bare atomic inversion except at $\chi = \pi/4$. Such connection between DS inversion and bare atomic inversion is the key factor in achieving unexpected inversion.

When state $|1\rangle$ and field L_1 are included, equality (15) can be broken and novel effects will occur. Under ideal DSCPT configuration ($\rho_{NC,NC} \approx 1$), the DS populations is better approximated by

$$\frac{\rho_{SS}}{\rho_{TT}} \approx \cot^2 \theta, \quad (17)$$

according to Eq.(5). Thus a DS inversion can be achieved for $\theta < \pi/4$ (i.e., $\Omega_T > \Omega_S$). Substitute (17) into (16) (along with $\rho_{SS} + \rho_{TT}=1$), we arrive at

$$\rho_{22} - \rho_{33} \approx \cos 2\chi \cdot \frac{\cot^2 \theta - 1}{\cot^2 \theta + 1}, \quad (18)$$

which is a concise prediction on the magnitude of bare atomic inversion assuming ideal DSCPT.

In Fig.4 we plot the steady-state inversion $\rho_{22} - \rho_{33}$ as a function of θ numerically [(a), using the procedure in Section 2] and analytically [(b), using Eq.(18)]. For a convenient comparison with existing studies, we have chosen $\Gamma_2 = 0.0025$ to represent a real Barium V-type atom spanned by $6s6p^1P_1$ ($|1\rangle$), $6s6p^3P_1$ ($|2\rangle$) and $6s6s^1S_0$ ($|3\rangle$). In all calculations we fix $\Omega_2 = 5$ and tune χ by varying Δ_2 . Within the range $0 < \theta < \pi/2$ $\sqrt{\Omega_T^2 + \Omega_S^2} = 1$ is kept by adjust Ω_1^\pm . Meanwhile, the two-photon resonance condition for DSCPT is met by choosing $\Delta_1 = \frac{1}{2}\Delta_2$ and $\delta = \frac{1}{2}\sqrt{\Delta_2^2 + \Omega_2^2}$. As is seen from Fig.4, the numerical calculation matches very well with the analytical approximation. The non-inverted to inverted transition always occurs at $\theta = \pi/4$ as predicted from Eq.(18). The highest inversion in Fig.4(a) is 0.73, which is much larger than 0.11 reported in [11], and is very close to the best value 0.77 obtained by intense numerical optimization in [12].

In the limit $\Omega_T/\Omega_S \rightarrow \infty$ ($\theta \rightarrow 0$) the bichromatic field L_1 reduces to a monochromatic one. Under such condition our model will be essentially the same as in [11], except that the analysis in Ref. [11] is based on first dressing the transition $|1\rangle - |3\rangle$ instead of $|2\rangle - |3\rangle$. Within their parameter range the magnitude of inversion is

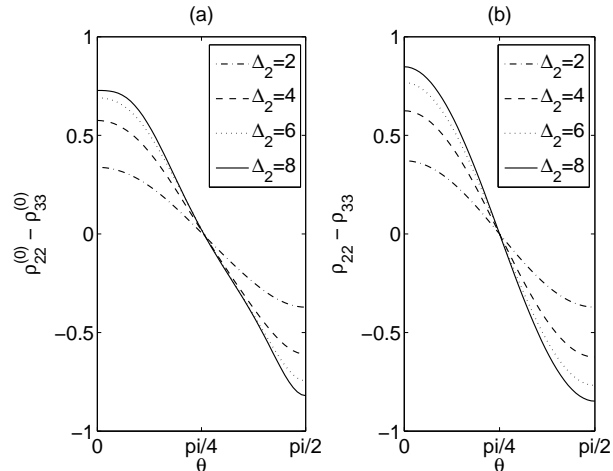


Figure 4. The steady-state inversion $\rho_{22} - \rho_{33}$ as a function of θ for several values of detuning Δ_2 , which correspond to $\chi = 0.6$ (dash-dotted), 0.45 (dashed), 0.34 (dotted) and 0.28 (solid). Plots in (a) and (b) are obtained by an exact numerical calculation and an approximate analytical method, respectively.

relatively poor, as is verified by later numerical simulations [12]. However, as shown by our analytical and numerical investigation, the inversion via DSCPT provide not only a better approaching to the optimal parameters but also a simpler understanding on the origin of the unexpected inversion.

3.3. LWI with and without hidden inversion

As an attractive approach for the generation of continuous-wave short-wavelength lasers, LWI in atomic systems has been well studied for many years. Thank to the various quantum interference channels available, multi-level systems are currently the workhorses for LWI. However, two-level system is still a good demonstration of the principles.

Two LWI regimes are well recognized for a coherently driven TLA: (i) gain via hidden inversion and (ii) gain without hidden inversion. In the first regime, although bare atomic population is not inverted, the net gain of a probe field can still be attributed to a hidden inversion (e.g., inversion in the DS basis). A typical example is the gain/absorption peak located at the left/right Rabi sideband for a *off-resonantly* driven TLA (see, the dotted line in Fig. 5), where the magnitude of gain/absorption is proportional to the DS population difference [19]. In the second regime, the probe gain originates from the coherent energy transfer between the two fields and no population inversion is found for any meaningful basis. An example is the probe gain in a *resonantly* driven TLA [see, Fig. 6(a)] [14]. Such gain profile cannot be attributed to hidden inversion since the DS population is now equalized. The gain in the second regime is generally much weaker than that in the first regime.

Aided with DSCPT, an interesting LWI via hidden inversion can be seen even when

the driving field is on-resonance with the TLA. In Fig. 5 we plot the probe gain for $\theta = 0$ (dashed line) and $\theta = \pi/2$ (solid line) respectively. In contrast to the LWI for an off-resonantly driven TLA, where the gain is always much weaker than the absorption, the probe gain/absorption peaks are now equal in magnitude. To explain the probe spectra, it is convenient to attribute the gain/absorption at the left (right) Rabi sideband to the DS transition $|T_n\rangle \rightarrow |S_{n-1}\rangle/|S_{n-1}\rangle \rightarrow |T_n\rangle$ ($|S_n\rangle \rightarrow |T_{n-1}\rangle/|T_{n-1}\rangle \rightarrow |S_n\rangle$). Recalling that the total gain/absorption for each Rabi transition is proportional to the corresponding DS population difference and the square of the associated dipole moment [which is proportional to $\sin^4 \chi$ ($\cos^4 \chi$) for the left (right) Rabi transition], the gain profile in Fig. 5 can be well understood for $\chi = \pi/4$. Another interesting feature takes place for $\theta = \pi/4$ (i.e., $\rho_{SS} = \rho_{TT}$), in this case no DS inversion exists at all. The probe gain under such condition is plotted in Fig. 6(b). As expected, such LWI without hidden inversion is much weaker than that shown via hidden inversion. In contrast to Fig. 6(a), the gain is now located at the *outer* sides rather than the *inner* sides of the two Rabi sidebands. Numerical calculations show (not shown here) a smooth evolution between Fig. 6(a) and (b) when Ω_T and Ω_S are gradually increased. Such difference in gain profile caused by increasing DS coherence is more or less connected with the *amplification by coherence* investigated in [21], however, to explore the detail of which is beyond the scope of the present paper.

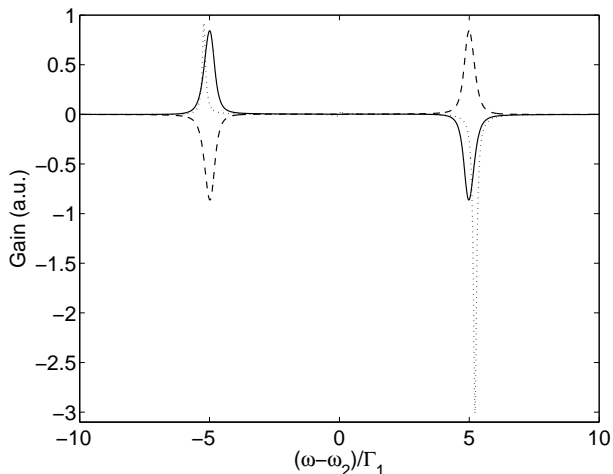


Figure 5. LWI via hidden inversion. The dotted line denotes the probe gain for a off-resonantly driven TLA, where an optimal detuning ($\Delta_2 = 1.5$, $\Omega_2 = 5$, $\Gamma_2 = 0.1$) is used for maximal gain [20]. LWI via DSCPT induced hidden inversion is plotted for $\theta = 0$ (dashed line) and $\theta = \pi/2$ (solid line), with parameters $\Delta_2 = 0$, $\Gamma_1 = 1$, $\Gamma_2 = 0.1$, $\Omega_2 = 5$, and $\sqrt{\Omega_T^2 + \Omega_S^2} = 0.5$.

4. Summary

We have shown that by using an auxiliary bichromatic field, CPT can be formed in the DS basis of a monochromatically driven TLA, using both a dressed-atom analysis

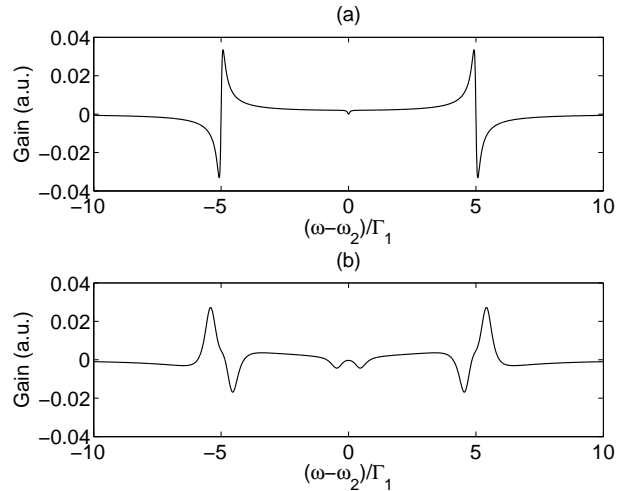


Figure 6. LWI without hidden inversion. The probe gain in (a) a resonantly driven TLA ($\Delta_2 = 0$, $\Omega_2 = 5$, $\Gamma_2 = 0.1$) and (b) a resonantly driven TLA with DSCPT ($\Omega_T = \Omega_S = 1$, $\Gamma_2 = 0.1$, $\Omega_2 = 5$, $\Delta_2 = 0$).

and a master equation calculation. The demonstrated DSCPT can be viewed as a new doorknob to manipulate a two-level system via its control over the DS populations. Examples of such manipulation are discussed in various applications, among which we show that the DSCPT induced unexpected inversion provides a new point of view to the origin of dynamically induced irreversibility, both qualitatively and quantitatively.

Acknowledgments

This work was supported by the PCSIRT, the SRFDP, the NFRPC Grant No. 2006CB921205, and the National Natural Science Foundation of China Grant No. 10625416 and No. 10534060.

References

- [1] Arimondo E 1996 *Progress in Optics* (XXXV) p 257
- [2] Bergmann K, Theuer H and Shore B W 1998 *Rev. Mod. Phys.* **70** 1003
Král P, Thanopoulos I and Shapiro M 2007 *Rev. Mod. Phys.* **79** 53
- [3] Fleischhauer M, Imamoglu A and Marangos J P 2005 *Rev. Mod. Phys.* **77** 633
Lukin M D 2003 *Rev. Mod. Phys.* **75** 457
- [4] Mompert J and Corbalan R 2000 *J. Opt. B: Quantum Semiclass. Opt.* **2** R7
- [5] Michaelis B, Emary C and Beenakker C W J 2006 *Europhys. Lett.* **73** 677
Groth C W, Michaelis B and Beenakker C W J 2006 *Phys. Rev. B* **74** 125315
Emary C 2007 *Phys. Rev. B* **76** 245319
- [6] Gray H R, Whitley R M and Stroud C R Jr *Opt. Lett.* **3** 218 (1978).
- [7] Allen L and Eberly J H 1987 *Optical Resonance and Two-Level Atoms* (New York: Dover).
- [8] Scully M O and Zubairy M S 1997 *Quantum Optics* (Cambridge: Cambridge University Press).
- [9] Cohen-Tannoudji C, Dupont-Roc J and Grynberg G 1998 *Atom-Photon Interaction: Basic Processes and Applications* (New York: Wiley)

- [10] Ficek Z and Rudolph T 1999 *Phys. Rev. A* **60** R4245
Yu C C, Bochinski J R, Kordich T M V, Mossberg T W and Ficek Z 1997 *Phys. Rev. A* **56** R4381
Rudolph T G, Freedhoff H S and Ficek Z 1998 *Phys. Rev. A* **58** 1296
Ficek Z and Freedhoff H S 1996 *Phys. Rev. A* **53**, 4275
- [11] Meduri K K, Wilson G A, Sellin P B and Mossberg T W 1993 *Phys. Rev. Lett.* **71** 4311
- [12] Hu X M and Peng J S 2000 *Chin. Phys. Lett.* **17** 200
- [13] Lezama A, Barreiro S, Lipsich A and Akulshin A M 1999 *Phys. Rev. A* **61** 013801
- [14] Mollow B R 1969 *Phys. Rev.* **188** 1969
Mollow B R 1972 *Phys. Rev. A* **5** 2217
- [15] Li P, Nakajima T and Ning X J 2006 *Phys. Rev. A* **74** 043408
- [16] Li X X, Hu X M, Shi W X, Xu Q, Guo H J and Li J Y 2006 *Chin. Phys. Lett.* **23** 340
- [17] Zhang J P, Xu J, Hernandez G, Hu X M and Zhu Y F 2007 *Phys. Rev. A* **75** 043810
- [18] Loudon R 1985 *Quantum Theory of Light* (Oxford: Oxford University Press) p 23
- [19] Wilson G A, Meduri K K, Sellin P B and Mossberg T W 1994 *Phys. Rev. A* **50** 3394
- [20] Wu F Y, Ezekiel S, Ducloy M and Mollow B R 1977 *Phys. Rev. Lett.* **38** 1077
- [21] Agarwal G S 1991 *Phys. Rev. A* **44** R28